Title

Osteogenic preconditioning in perfusion bioreactors improves vascularization and bone formation by human bone marrow aspirates.

Journal

Science advances, 6(7)

ISSN

2375-2548

Authors

Harvestine, JN
Gonzalez-Fernandez, T
Sebastian, A
et al.

Publication Date

2020-02-01

DOI

10.1126/sciadv.aay2387

Peer reviewed

HEALTH AND MEDICINE

Osteogenic preconditioning in perfusion bioreactors improves vascularization and bone formation by human bone marrow aspirates

J. N. Harvestine[1], T. Gonzalez-Fernandez[1], A. Sebastian[2], N. R. Hum[2], D. C. Genetos[3], G. G. Loots[2], J. K. Leach[1,4]*

Cell-derived extracellular matrix (ECM) provides a niche to promote osteogenic differentiation, cell adhesion, survival, and trophic factor secretion. To determine whether osteogenic preconditioning would improve the bone-forming potential of unfractionated bone marrow aspirate (BMA), we perfused cells on ECM-coated scaffolds to generate naïve and preconditioned constructs, respectively. The composition of cells selected from BMA was distinct on each scaffold. Naïve constructs exhibited robust proangiogenic potential in vitro, while preconditioned scaffolds contained more mesenchymal stem/stromal cells (MSCs) and endothelial cells (ECs) and exhibited an osteogenic phenotype. Upon implantation into an orthotopic calvarial defect, BMA-derived ECs were present in vessels in preconditioned implants, resulting in robust perfusion and greater vessel density over the first 14 days compared to naïve implants. After 10 weeks, human ECs and differentiated MSCs were detected in de novo tissues derived from naïve and preconditioned scaffolds. These results demonstrate that bioreactor-based preconditioning augments the bone-forming potential of BMA.

INTRODUCTION

With nearly 400 currently active and/or recruiting clinical trials in the United States (www.clinicaltrials.gov, accessed 16 May 2019), bone marrow–derived mesenchymal stem/stromal cells (MSCs) are under widespread clinical investigation for their regenerative capacity. Bone marrow aspirate (BMA) is a readily available source of hematopoietic and mesenchymal progenitor cells for autologous cell therapy. Current point-of-care devices concentrate bone marrow for direct injection, yet MSCs only comprise 0.01% of nucleated cells from the bone marrow (*1*). Therefore, extended ex vivo culture is necessary to produce a sufficient number of MSCs for clinical use. However, the high costs associated with Good Manufacturing Practices and increased regulatory burden introduced by in vitro culture motivate the development of alternative strategies to use BMA.

Preconditioning of cells before transplantation provides critical stimuli to guide cell function, and several groups report that preconditioning MSCs in vitro improves their survival and potential for tissue formation (*2*). For example, preconditioning MSCs with tetrandrine-activated secretion of prostaglandin E2, an immunosuppressive molecule, resulted in decreased inflammation when cells were implanted in a mouse model (*3*). Hypoxic preconditioning of MSCs improved cell survival in a subcutaneous site (*4*), angiogenesis in hindlimb ischemia (*5*), and bone formation in critical-sized femoral defects (*6*). The bone-forming potential of cells from lipoaspirates and BMA is increased when cells are expanded in perfusion bioreactors compared to traditional monolayer culture (*7*, *8*). Additional studies demonstrate that tissue aspirates have osteogenic potential when implanted immediately after isolation with minimal in vitro manipulation (*9*). An intraoperative procedure to apply autologous cells for tissue regeneration is the preferred strategy for clinical translation. However, there are limited studies to determine whether osteogenic preconditioning of BMAs before implantation will improve bone formation. Furthermore, the interplay of soluble (e.g., inductive factors) and substrate-mediated cues (e.g., extracellular matrices) on BMA for bone formation in three-dimensional (3D) perfusion culture is unknown.

Extracellular matrix (ECM) provides soluble and insoluble cues to direct cell adhesion, migration, differentiation, and tissue-specific functions (*10*). Bottom-up biomaterial design efforts aim to recapitulate cellular responses to key ECM components (*11*, *12*). However, these approaches fail to mimic the diverse and complex composition of cell-derived ECM, thereby restricting the advantageous contribution of diverse ligands to direct cell fate. Cell-secreted ECM generated in vitro maintains the complex nature of ECM and has been used as a surface coating of 3D materials to direct osteogenic differentiation for bone tissue engineering (*13*, *14*). In combination with perfusion bioreactors, ECM on ceramic scaffolds successfully sequestered cells from BMA and recapitulated a bone marrow niche capable of supporting both differentiated and hematopoietic progenitor cells after isolation (*15*). We recently demonstrated that ECM-coated scaffolds enrich endothelial and MSC subpopulations from BMA, but we did not observe differences in bone formation when scaffolds were implanted into an ectopic site (*16*). Whether preconditioning BMA in the presence of ECM affects the osteogenic potential of the construct is unknown.

We hypothesized that osteogenic preconditioning of cells from BMA on an ECM-coated scaffold would improve bone formation upon implantation (Fig. 1). To investigate this hypothesis, we assessed the ability of ECM-coated scaffolds to sequester cells from unprocessed BMA. We then examined the effect of in vitro preconditioning in a perfusion bioreactor to prompt neovascularization and bone regeneration versus nonconditioned BMA in an orthotopic bone defect model.

[1]Department of Biomedical Engineering, University of California, Davis, Davis, CA 95616, USA. [2]Physical and Life Sciences, Lawrence Livermore National Laboratory, Livermore, CA 94550, USA. [3]Department of Anatomy, Physiology, and Cell Biology, School of Veterinary Medicine, University of California, Davis, Davis, CA 95616, USA. [4]Department of Orthopaedic Surgery, School of Medicine, UC Davis Health, Sacramento, CA 95817, USA.
*Corresponding author. Email: jkleach@ucdavis.edu

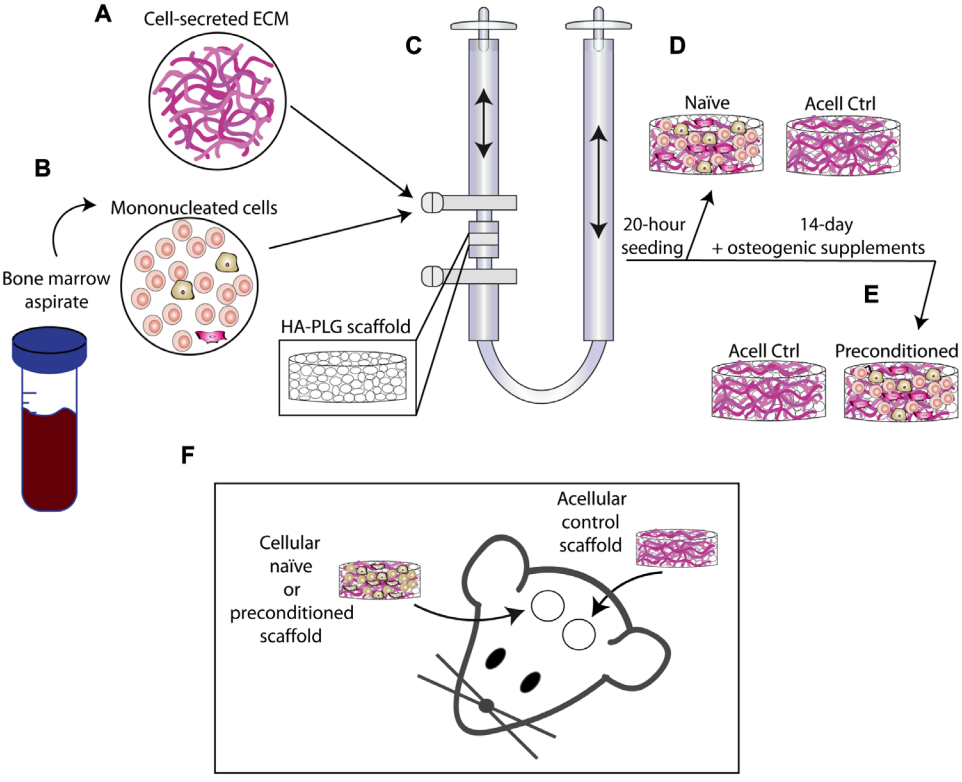

Fig. 1. Schematic of experimental design. (**A**) Medium containing cell-secreted ECM was mixed with (**B**) mononucleated cells from BMA and seeded onto (**C**) HA–poly(lactide-*co*-glycolide) (PLG) scaffolds using a perfusion bioreactor. After 20 hours of perfusion, (**D**) naïve scaffolds were retrieved, and (**E**) preconditioned scaffolds were perfused with culture medium containing osteogenic supplements for 13 additional days. (**F**) Scaffolds were implanted into 3.5-mm bilateral calvarial defects.

RESULTS

Preconditioning promotes the expansion of MSCs and endothelial cells from BMA

Scaffolds maintained structural integrity and overall morphology after both culture durations (20 hours and 14 days) (Fig. 2A). We used flow cytometry to determine the immunophenotype of cells before and after culture (Fig. 2, B to D). Myeloid cells ($CD45^+$ $CD31^-$) constituted approximately 80% of cells from fresh BMA, and this proportion was maintained over the 20-hour perfusion ($P = 0.9175$) to produce naïve constructs (Fig. 2B). However, this proportion was reduced over 14 days of osteogenic preconditioning to approximately 6% of cells ($P < 0.0001$). The fraction of MSCs ($CD73^+CD90^+$ $CD45^-$) in the fresh BMA (0.2%) was increased to 0.8 and 6.5% in naïve ($P = 0.8659$) and preconditioned ($P = 0.001$) constructs, respectively (Fig. 2C). We also observed a 17-fold increase in the percentage of endothelial cells (ECs; $CD31^+CD45^-$) during in vitro preconditioning ($P = 0.003$) (Fig. 2D). Scanning electron microscopy (SEM) revealed that cells on naïve constructs were often rounded and located along the periphery of pores, while cells in preconditioned grafts exhibited pore-spanning, stretched morphologies (Fig. 2E).

Duration of bioreactor preconditioning influences construct phenotype

We performed RNA sequencing (RNA-seq) on cells retrieved from BMA, naïve, and preconditioned constructs to determine how bioreactor seeding and preconditioning affected cell phenotype. We also performed quantitative polymerase chain reaction (qPCR) to validate the expression of key osteogenic and angiogenic genes. In agreement with the flow cytometry data, preconditioning significantly reduced the expression of genes associated with immune and inflammatory events expressed by myeloid-derived cells (fig. S1 and table S1). Critical genes associated with osteogenic differentiation—*COL1A1*, *COL1A2*, *MGP*, *SPP1*, *PHEX*, and *BMP-2*—were significantly up-regulated in preconditioned constructs (Fig. 3A, osteogenesis heatmap, and table S2) compared to naïve scaffolds. *RUNX2*, the master transcription factor for osteogenesis, was also up-regulated in preconditioned constructs compared to naïve constructs, yet it had the highest expression in BMA (table S2). Expression of *BGLAP*, the gene encoding for osteocalcin (OCN), was extremely low in both naïve and preconditioned constructs, suggesting that the preconditioned cells are more likely immature osteoblasts at day 14. Expression of several genes associated with vasculature development, including *VEGFC*, *PDGFA*, *PGF*, *PDPN*, and *EFNB2*, was significantly up-regulated in preconditioned scaffolds compared to naïve constructs (Fig. 3A, vasculature development heatmap, and table S3). However, expression of *VEGFA*, encoding for the potent angiogenic protein vascular endothelial growth factor (VEGF), was greatest in naïve constructs (table S3).

qPCR confirmed RNA-seq expression of *RUNX2*, *SP7*, and *BGLAP* (Fig. 3, C to E). In contrast, genes associated with later stages of osteogenic differentiation, *IBSP*, *COL1A1*, and *BMP-2*, were up-regulated in preconditioned constructs (Fig. 3, F to H) compared to naïve scaffolds. In agreement with both RNA-seq and qPCR results (Fig. 3B), VEGF secretion was greater in naïve constructs (Fig. 3I), while bone morphogenetic protein-2 (BMP-2) secretion was greater in preconditioned constructs (Fig. 3K). Despite low *BGLAP* expression

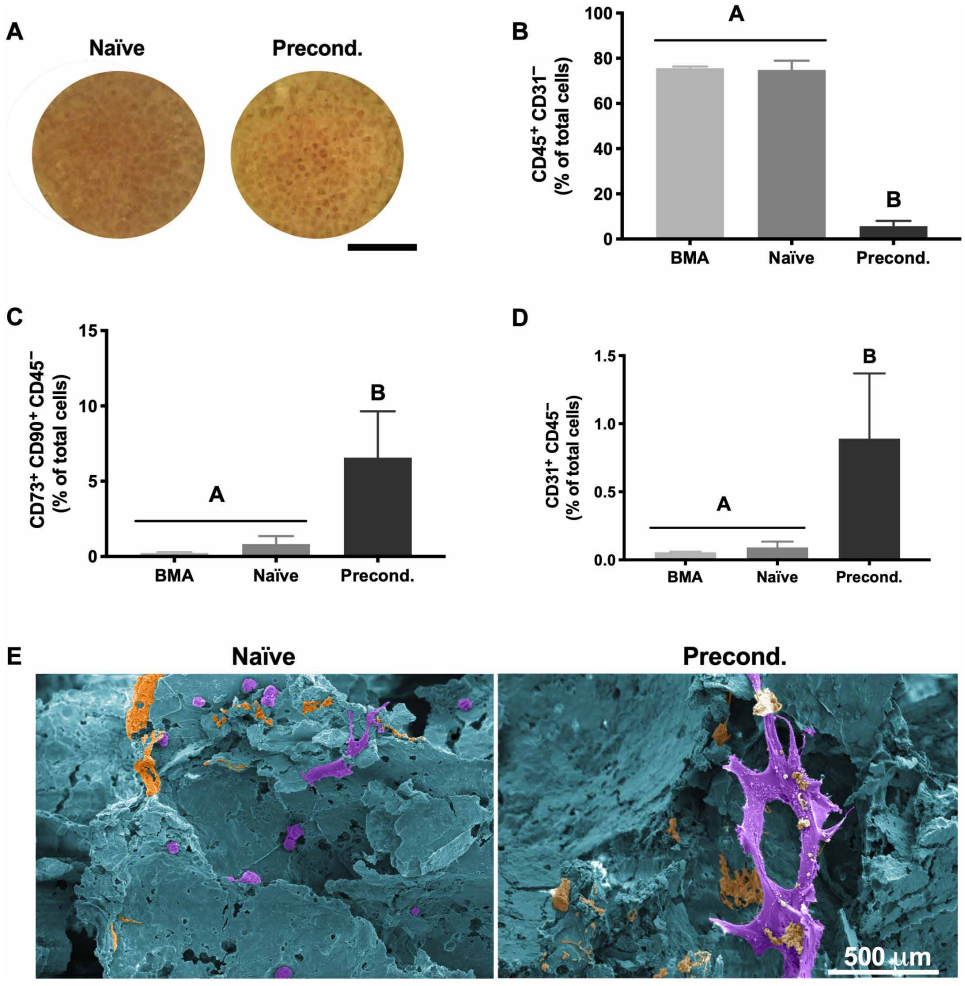

Fig. 2. Preconditioning increases MSC and EC content in osteogenic grafts. (**A**) Gross morphology images of (left) naïve and (right) preconditioned grafts after culture. Scale bar, 4 mm. (**B** to **D**) Percentage of cells that are (B) hematopoietic ($CD45^+CD31^-$), (C) endothelial ($CD31^+CD45^-$), and (D) mesenchymal ($CD73^+CD90^+CD45^-$) in origin ($n = 4$ to 5). (**E**) Representative SEM images of (left) naïve and (right) preconditioned grafts false-colored to show cells in purple, ECM in orange, and scaffold in blue. Scale bar, 500 μm.

in both naïve and preconditioned constructs, we observed greater OCN secretion by cells on preconditioned constructs (Fig. 3J). Immunohistochemistry revealed greater OCN presence in the ECM of preconditioned grafts (Fig. 3M). All constructs were coated with cell-secreted ECM during cell seeding, evidenced by positive staining with picrosirius red in naïve grafts (Fig. 3L, left). Entrapped cells continued to deposit a collagenous ECM during preconditioning evidenced by greater collagen content in preconditioned grafts (Fig. 3L, right). We analyzed the mineral content of the naïve and preconditioned groups at day 14 of in vitro culture through micro-computed tomography (micro-CT) and Alizarin Red staining of mineral deposition. Mineral content established by bone volume (BV) and calcium staining was visibly greater in the naïve group than in the preconditioned scaffolds, likely due to hydroxyapatite (HA) degradation during preconditioning (fig. S2).

Preconditioned grafts improve neovascularization of implants

Both naïve and preconditioned constructs exhibited increasing levels of vascularization during the first 2 weeks after implantation when followed with laser Doppler perfusion imaging (LDPI; Fig. 4, A and C). At day 14, defects treated with preconditioned grafts exhibited significantly increased perfusion compared to defects filled with naïve constructs ($P = 0.042$). The greatest level of perfusion across the whole study was observed at this time point. Perfusion in defects treated with naïve grafts peaked at day 28 and was significantly higher than those treated with preconditioned scaffolds at day 35. At the conclusion of the study (day 70), perfusion was similar in both groups. In agreement with LDPI, we observed increased vessel density in preconditioned grafts ($P = 0.0017$) when evaluating histology of explants at 2 weeks (Fig. 4B). Staining against human-specific CD31 revealed the presence of human ECs in both naïve and preconditioned implants, yet blood vessels of human origin were only observed in preconditioned grafts (Fig. 4D).

Hematoxylin and eosin (H&E)–stained sections revealed cellular infiltration into both naïve and preconditioned constructs after 2 weeks (Fig. 4E). Patches of early woven bone and osteoid were observed in sections stained with Masson's trichrome (Fig. 4F). Immunostaining for OCN revealed more prominent staining in naïve constructs compared to preconditioned constructs, which more closely

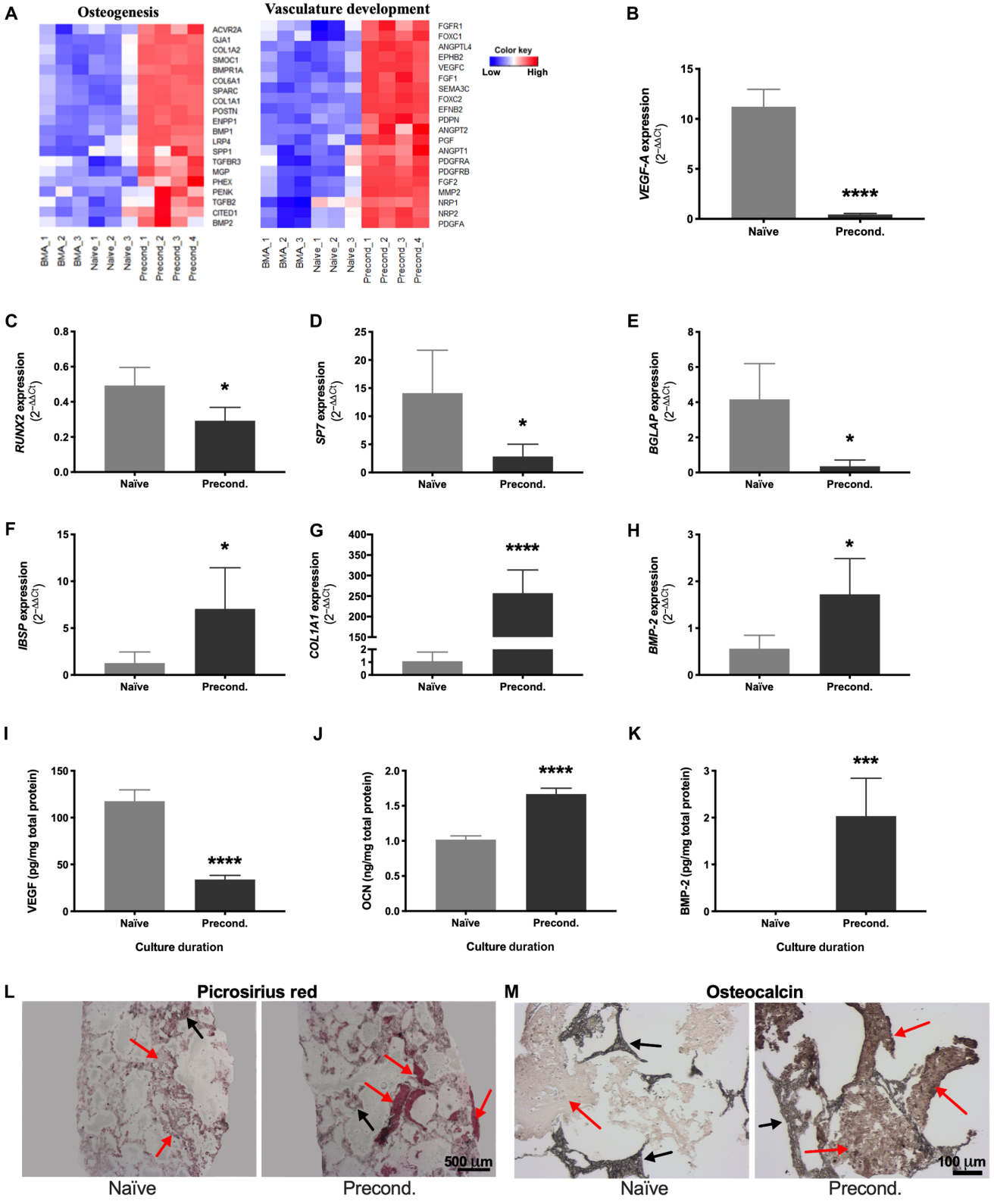

Fig. 3. In vitro culture duration modulates phenotype of entrapped cells. (**A**) Heatmaps representing RNA-seq data of 20 key regulators of osteogenesis and vascular development up-regulated in preconditioned compared to naïve constructs ($n = 3$ to 4). (**B** to **H**) Relative expression of genes involved in proangiogenic potential and osteogenic differentiation as a function of duration in perfusion culture ($n = 5$). (**I**) Proangiogenic and (**J** and **K**) osteogenic protein secretion ($n = 5$ to 6). Histological sections stained with (**L**) picrosirius red (scale bar, 500 μm) and (**M**) anti-OCN (scale bar, 100 μm). Red arrows denote positive staining, and black arrows denote scaffold. $^*P < 0.05$, $^{***}P < 0.001$, $^{****}P < 0.001$.

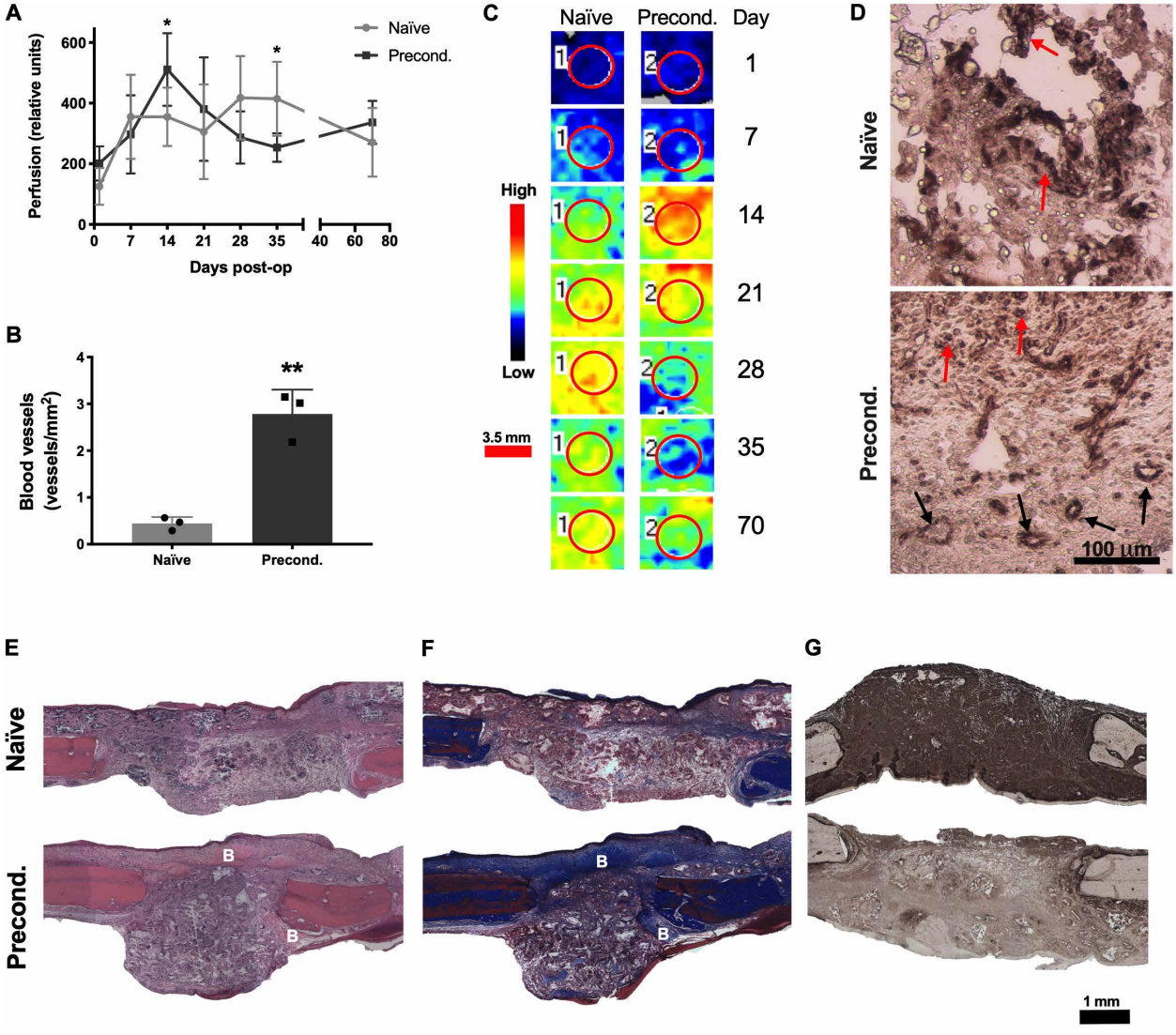

Fig. 4. Preconditioned grafts enhance early vascularization. (**A**) Raw perfusion values from LDPI ($n = 6$). (**B**) Quantification of vessel density ($n = 3$). (**C**) Representative LDPI images color mapped to reveal the magnitude of perfusion quantified from the defect area denoted by a red circle. Scale bar, 3.5 mm. (**D**) Immunostaining for human CD31. Black arrows denote vessel structures, and red arrows denote positive staining for non–vessel-forming cells. Scale bar, 100 μm. (**E**) Hematoxylin and eosin (H&E), (**F**) Masson's trichrome, and (**G**) anti-OCN staining. Scale bar, 1 mm. New woven bone is denoted B. $^*P < 0.05$, $^{**}P < 0.01$.

resembled the staining present in the native bone present on the defect margins (Fig. 4G).

Preconditioning improves bone formation

Bioreactor culture duration did not alter the resultant BV or average mineral density in acellular constructs, and the addition of cells in naïve constructs did not enhance bone formation over acellular controls. Significant increases in BV ($P = 0.019$) (Fig. 5A) and corresponding values for average mineral density throughout the defects ($P = 0.041$) were observed in preconditioned constructs compared to all other groups. However, the newly formed bone mineral density was similar across all groups ($P > 0.478$) (Fig. 5B). Representative micro-CT images demonstrate uniform bone formation throughout the surface and volume of preconditioned implants compared to naïve implants that exhibit islands of mineralized tissue (Fig. 5C). We observed a moderate correlation between the day 14 perfusion values versus BV ($P = 0.01$, $r^2 = 0.48$) and average mineral density ($P = 0.01$, $r^2 = 0.49$) (Fig. 5D, left). When the implant with the greatest perfusion is compared to the implant with the least perfusion, we observed an appreciable increase in bone formation (Fig. 5D, right).

Histological staining confirmed new bone formation in sections stained with H&E and Masson's trichrome (Fig. 6, A and B). Preconditioned scaffolds resulted in better integration with host bone compared to naïve scaffolds (fig. S3). Staining with human-specific anti-CD31 revealed the presence of human ECs and human-derived vasculature in both naïve and preconditioned implants after 10 weeks (Fig. 6C), unlike 2-week explants that did not include human $CD31^+$ cells within the vasculature of naïve constructs. Similarly, staining with human-specific anti–distal-less homeobox 5 (DLX5), a marker of MSC osteogenesis (*17*), revealed the presence of human-derived MSCs undergoing osteogenic differentiation in both the naïve and preconditioned implants after 10 weeks of in vivo implantation

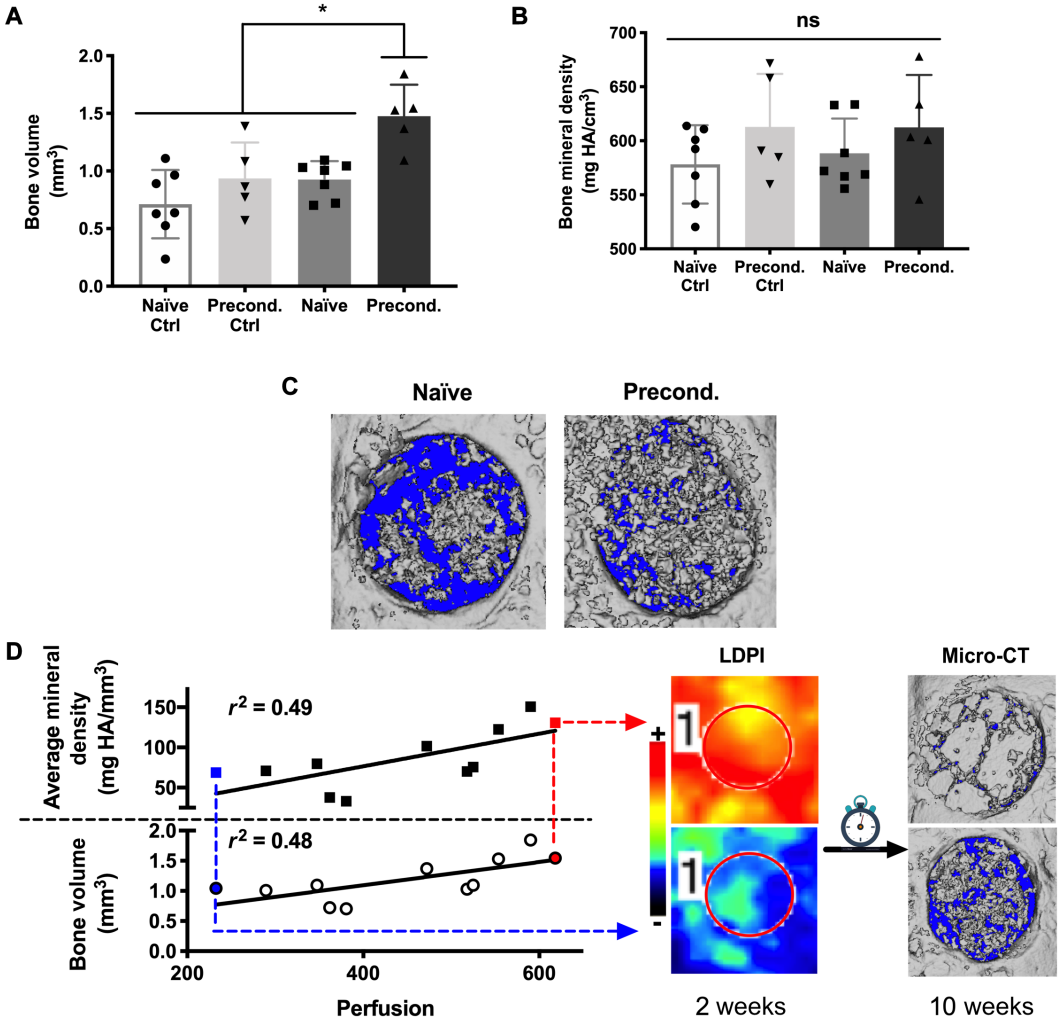

Fig. 5. Early vascularization correlates with bone formation by preconditioned grafts. (**A**) BV. (**B**) Bone mineral density. For (A) and (B), $n = 5$ for controls and $n = 7$ for experimental groups (*$P < 0.05$). (**C**) Representative micro-CT images of defects at 10 weeks after implantation. (**D**) Correlations between perfusion at 14 days and 10-week BV ($P = 0.01$, $r^2 = 0.48$) and bone mineral density ($P = 0.01$, $r^2 = 0.49$). Lowest and highest perfusion values are denoted with blue and red points, respectively, and connected via arrows to corresponding LDPI and micro-CT images.

(Fig. 6, D to G). These results confirm the presence of the transplanted human cells and their essential role in the development of new vasculature and bone tissue at the site of implantation.

DISCUSSION

The delivery of bone marrow–derived MSCs to augment tissue repair is at the forefront of regenerative medicine for orthopedic indications, including avascular necrosis of the femoral head (*18*) and cartilage lesions (*19*). Current technologies concentrate nucleated cells from BMA but are unable to select for MSCs that have osteogenic potential and a complex secretome that recruits endogenous cells for tissue regeneration. Clinical outcomes demonstrate a positive correlation between the number of colony forming units and bone formation by autologous BMA injection (*20*), yet MSCs represent 0.01% of nucleated cells from BMA (*1*) and require culture expansion to generate clinically relevant cell numbers. Bone formation has been reported when implanting tissue aspirates after minimal ex vivo culture and cell expansion using perfusion bioreactors (*7*, *8*, *21*). However, a direct comparison of uncultured and preconditioned BMA has not been reported. Here, we describe the effect of osteogenic preconditioning via perfusion bioreactor culture on the bone-forming capacity of BMA.

Bioreactors are an effective and scalable strategy for MSC expansion compared to traditional monolayer culture (*7*, *22*, *23*). Beyond expansion, perfusion flow-induced shear stress promotes an osteogenic phenotype (*24*) and deposition of a mineralized ECM by MSCs (*25*, *26*). Thibault *et al.* (*14*) reported that murine bone marrow–derived MSCs cultured in short-term perfusion culture deposited an ECM rich in collagen I, HA, and matrix-remodeling proteins. Perfusion culture can be used to populate implantable biomaterials with cells from tissue aspirates to locally concentrate and activate cells in the defect site. In this study, naïve constructs maintained similar cell composition to freshly isolated BMA and expressed high levels of transcripts associated with myeloid cell fate. In contrast, preconditioned constructs contained fewer hematopoietic cells and increased proportions of both MSCs and ECs. Consistent with cells undergoing osteogenic differentiation, preconditioning resulted in high expression of several markers of

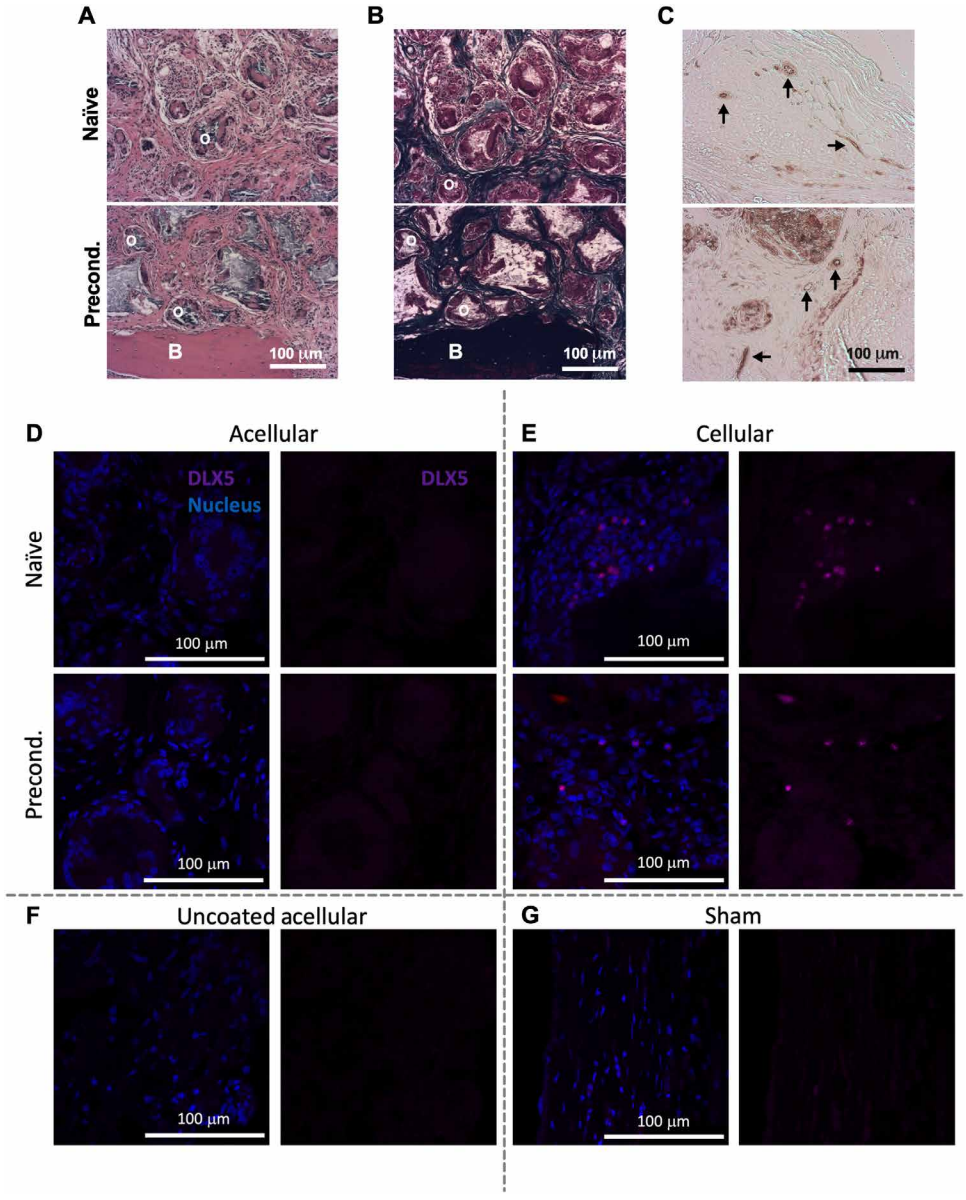

Fig. 6. Human ECs and MSCs engraft into new bone tissue. (**A** to **C**) Histological sections stained with (A) H&E, (B) Masson's trichrome, and (C) anti-human CD31. B and O denote new bone and osteoid, respectively, and black arrows denote vasculature of human origin. Scale bars, 100 μm. (**D** to **G**) Immunofluorescence staining of histological sections for anti-human DLX5 (magenta) and cell nucleus (blue). (D and E) (Top) Naïve and (bottom) preconditioned (D) acellular and (E) BMA-loaded scaffolds compared to (F) uncoated acellular and (G) sham controls. Scale bars, 100 μm.

osteogenesis, yet the molecular profiling suggested that osteoblasts within these constructs were immature. Immunohistochemistry, however, showed increased secretion of OCN that could be indicative of either a slower protein turnover or a slightly more mature stage of osteoblasts in these constructs. Preconditioned constructs had reduced expression and secretion of VEGF-A yet expressed several other pro-angiogenic genes at a higher level. It is unclear which differentiation stage the MSCs within the BMA have achieved after 14 days, but this is further complicated by the heterogeneity of the aspirate, donor variability, and the inability to specifically analyze changes in differentiation stage of subpopulations within the graft with the studies as designed. RNA-seq data demonstrate the increasing expression of multiple osteogenic genes in the preconditioned scaffolds compared to naïve scaffolds, providing further evidence that cells within the graft are undergoing osteogenic differentiation. We also demonstrate by RNA-seq that many genes associated with vascular development are up-regulated in preconditioned scaffolds, which is in contrast to data establishing the inverse relationship between osteogenesis and angiogenic potential in human MSCs (*27*, *28*). These results indicate that 14 days of osteogenic preconditioning in perfusion bioreactors is sufficient to shift cellular differentiation toward bone-forming cells, yet the osteoblasts are still immature. A longer preconditioning span may further enhance osteogenesis of these constructs.

HA provides an osteoconductive surface and is widely used in bone regeneration (*7*, *29*, *30*). Moreover, HA scaffolds coated with cell-derived ECM were recently used to recapitulate the bone marrow

niche and support hematopoiesis by fresh BMAs in vitro using perfusion bioreactors (*15*). For clinical application, it is important that materials are easily handled and amenable to modifications using tools readily available in the operating theater. On its own, HA is brittle and difficult to cut to the shapes and sizes needed for irregular defects. In this study, we fabricated a composite scaffold with a 2.5:1 weight ratio of HA to poly(lactide-*co*-glycolide) (PLG) microspheres, a Food and Drug Administration (FDA)–approved biodegradable polymer. In previous studies, this formulation promoted osteogenic differentiation concomitant with sustained VEGF secretion by MSCs in vitro and robust bone formation in vivo (*31*). The formation of scaffolds from PLG microspheres provides additional opportunities to incorporate biomacromolecules with controlled release kinetics to instruct cell function (*32*). Mineral content was reduced in preconditioned scaffolds compared to naïve constructs, likely due to HA degradation during the culture period. Despite the lack of mineralization at the time of implantation, preconditioned constructs induced superior healing in the calvarial defect model.

The necessity of revascularization during bone regeneration is well characterized, further motivating treatments that promote efficient vessel infiltration. VEGF-releasing PLG scaffolds successfully increased vessel density and resulted in bone regeneration of irradiated calvarial defects (*32*). Delivery of culture-expanded MSCs with various EC populations also improved vascularization and subsequent bone formation (*33*, *34*). This successful approach requires isolation of ECs from a secondary compartment, and it would be advantageous to deliver MSCs and ECs derived from the same tissue aspirate. However, MSCs and ECs represent a very small fraction of cells from BMA, and strategies to simultaneously expand both populations are lacking, motivating the need for strategies to sequester and promote expansion of these cells from BMA.

Cell-derived ECM is a biomimetic platform that increases MSC adhesion, survival, proliferation, trophic factor secretion, and osteogenic differentiation of associated MSCs (*13*, *25*, *35*). Cell-derived ECM was an effective material to retain endothelial and accessory cells from lipoaspirates and promote osteogenic differentiation within the resultant heterogenous cell population (*36*). In this study, we sought to determine whether preconditioning BMA before implantation was sufficient to increase bone formation. Datta *et al.* (*37*) reported the benefit of in vitro–generated ECM when perfusing and decellularizing scaffolds as a platform for MSC osteogenic differentiation. ECM produced in monolayer culture should be more consistent in composition than ECM deposited on constructs under perfusion that experience variation in shear stress and nutrient availability. The ECM used herein has been well characterized and is consistent across several donors. We and others have evaluated the impact of in situ ECM-coated scaffolds, demonstrating that more mature osteogenic grafts generated in vitro translate to improved bone formation in vivo. By coating scaffolds with ECM before preconditioning, we sought to accelerate this process. In agreement with our previous study (*36*), preconditioning of BMA via perfusion culture in the presence of ECM successfully retained and expanded the endothelial population concomitant to osteogenic differentiation by MSCs. Preconditioned constructs exhibited increased secretion of BMP-2, a potent osteoinductive molecule produced by ECs in coculture (*29*, *38*). The established synergy between MSC and EC populations in coculture improved EC vasculogenic capacity upon implantation (*39*) and improved MSC engraftment and regenerative capacity (*40*). In agreement, we observed persistence and engraftment of implanted ECs and MSCs throughout the 10-week study. ECs were observed within the lumen of vessel structures, and MSCs were positive for osteogenic differentiation marker, DLX5, demonstrating respective functional roles during new tissue formation. These data demonstrate that MSCs can directly participate in bone formation when provided appropriate cues and are not limited only to trophic factor secretion.

The pivotal role of angiogenesis during endochondral ossification (*41*) and intramembranous ossification (*32*) is well established. Despite limited VEGF expression and secretion, preconditioned implants resulted in robust vascular infiltration within 2 weeks in vivo. Moreover, we observed human-derived vasculature after 2 weeks in vivo, indicating that implanted ECs participated in neovascularization to quickly perfuse preconditioned constructs. Despite greater proangiogenic potential in vitro, naïve grafts exhibited maximum perfusion 2 weeks later at 28 days after implantation. Upon explantation at the conclusion of the study, we observed human cells within the vasculature of both naïve and preconditioned implants, indicating that ECs implanted in naïve constructs also participated in vessel formation. Even in preconditioned constructs, ECs represented a relatively small fraction of implanted cells, and the presence of human ECs after 10 weeks in vivo demonstrates prolonged cell survival and engraftment into newly formed tissue. Furthermore, early vascularization correlated to increased bone formation, suggesting that invading vasculature played a key role in bone formation. Preconditioned scaffolds were better integrated with host bone compared to naïve constructs. These data indicate that preconditioning increased the rate of vascular infiltration into implanted scaffolds. However, without more frequent sample collections, these data are insufficient to fully describe the contribution of vascular pruning and remodeling after initial vascular infiltration on resultant bone regeneration. Future studies evaluating these interactions are merited to better understand the interplay between vascular maturation and bone formation.

Healing within these subcritical-sized defects was expected over the course of the study, and the observed differences may reflect changes to the rate of healing as a result of preconditioning. For example, samples were stained for the presence of OCN both before and after implantation to assess the progression of osteogenic matrix deposition during healing. We observed strong staining for OCN in the ECM of preconditioned constructs before implantation and naïve implants after 14 days in vivo. In contrast, OCN staining decreased in preconditioned implants in vivo, which appeared more similar to the native bone at the defect margins. However, *BGLAP* expression, the gene encoding for OCN, was low in both naïve and preconditioned scaffolds in vitro. The discrepancy in *BGLAP* transcript expression, identified by RNA-seq data and confirmed by qPCR, versus protein levels identified by enzyme-linked immunosorbent assay (ELISA) and immunohistochemistry was initially puzzling. Reduced *BGLAP* expression could result from the heterogeneous population of cells within the construct, although that may not explain the reductions that were also observed by RNA-seq. RNA-seq demonstrates the overwhelming evidence that osteogenic genes are more highly upregulated with increasing culture time in perfusion. Transcriptional regulation of *BGLAP* is complex, revealing a species-specific response to vitamin D3 (*42*) and differential transcriptional versus post-transcriptional regulation depending on cell phenotype, with transcription outpacing protein product in immature osteoblasts, whereas protein synthesis is greater than transcription in mature osteoblasts (*43*). As scaffolds undergo continued remodeling in vivo, OCN incorporated within the scaffold during preconditioning was likely

liberated from the scaffold. The occurrence of remodeling in vivo is evident by the reduction in BV in naïve scaffolds at the conclusion of the study compared to preimplantation, wherein BV decreased from ~9 mm^3 (fig. S2A) to ~0.6 mm^3 (Fig. 5A). Conversely, there was little mineral content in preconditioned scaffolds upon implantation (fig. S2A), whereas robust BV (~1.5 mm^3) was evident at the conclusion. We also observed earlier neovascularization and implant perfusion in preconditioned implants, suggesting that preconditioning accelerated the rate of healing in vivo. While we observed angiogenic and osteogenic advantages due to preconditioning over the course of this study, it is difficult to predict whether these advantages would improve overall quality of bone formation after complete healing.

To our knowledge, this is the first report that directly compares the bone-forming potential of freshly isolated versus preconditioned human BMA in an orthotopic bone defect. From a translational perspective, it is advantageous to collect and deliver autologous cells during a single procedure without the need for ex vivo culture. However, the emergence of FDA-approved tissue engineering products such as MACI (Vericel Corporation, Cambridge, MA)—in which autologous chondrocytes are collected, shipped off-site, cryopreserved, expanded, and then reimplanted into the patient—demonstrates that these strategies are clinically and commercially feasible if they add therapeutic value. In this study, a relatively short in vitro culture duration significantly improved vascularized bone formation by BMA. Preconditioned grafts contained increased numbers of MSCs, and cells on these constructs expressed genes and deposited ECM consistent with osteogenic differentiation before implantation. Therefore, it is difficult to decouple the effects of delivering osteogenically primed MSCs versus simply delivering a larger number of MSCs to the defect site. However, transplantation of larger numbers of cells can yield diminishing returns due to massive cell death and insufficient nutrient availability. Furthermore, craniofacial bones heal via intramembranous ossification that relies on differentiating osteoprogenitor cells such as those present in preconditioned implants to mineralize the tissue. Long bones in the skeleton are formed and undergo repair via endochondral ossification, which requires the formation of a cartilaginous template before vascular infiltration and mineralization. The implantation of hypertrophic cartilaginous constructs, achieved over 3 to 6 weeks in culture, has successfully achieved vascularized bone regeneration in long bones (*30*, *44*). In contrast to the preconditioning performed here, which delivered ECs and MSCs to the defect site for rapid vascularization, preconditioning strategies that instruct the formation of a hypertrophic cartilage phenotype may prove more successful in long bone regeneration. Therefore, an optimal preconditioning regimen for concomitant chondrogenic and osteogenic preconditioning of MSCs and ECs before implantation into long bone defects merits further study. While these comparative studies are beyond the scope of this work, our results herein demonstrate that preconditioning of BMA on ECM-coated scaffolds generates a robust osteogenic graft containing a heterogeneous population of human cells that enhances bone healing.

MATERIALS AND METHODS

ECM production

Human bone marrow–derived MSCs (Lonza, Walkersville, MD) were used without further characterization. MSCs were expanded until use at passages 5 and 6 in minimum essential medium–α [α-MEM; with L-glutamine and without ribo/deoxyribonucleosides (Invitrogen, Carlsbad, CA)] supplemented with 10% fetal bovine serum (FBS; Atlanta Biologicals, Flowery Branch, GA) and 1% penicillin (10,000 U ml^{-1}) and streptomycin (10 mg ml^{-1}; Mediatech, Manassas, VA) (P/S). Cell-secreted ECMs were prepared as we described (*28*, *35*, *45*, *46*). Briefly, MSCs were seeded at 50,000 cells cm^{-2} and cultured in medium supplemented with ascorbate 2-phosphate (50 μg ml^{-1}) for 10 days with medium changes every 2 to 3 days. After culture, monolayers were washed with phosphate-buffered saline (PBS), and cells were removed using a detergent-based solution, followed by deoxyribonuclease (Sigma-Aldrich, St. Louis, MO) treatment (37°C for 1 hour) to remove 99.9% of DNA content from culture after decellularization (*45*). Decellularized ECM was washed three times with PBS and mechanically dislodged from culture flasks using a cell scraper. Total protein within the collected ECM was quantified using a bicinchoninic acid protein assay (Thermo Fisher Scientific, Rockford, IL). ECM solutions were frozen in 0.02 N acetic acid at −20°C until use.

Composite scaffold fabrication

Scaffolds were fabricated using a gas foaming/particulate leaching method as previously described (*16*, *31*, *47*). Microspheres composed of PLG (85:15; DLG 7E; Lakeshore Biomaterials, Birmingham, AL) were prepared using a double-emulsion process and lyophilized to form a free-flowing powder. Lyophilized microspheres (9.2 mg) were combined with 23.1 mg of HA crystals (particle size, 100 nm; Berkeley Advanced Biomaterials, Berkeley, CA) and 175.6 mg of NaCl (300 to 500 μm in diameter) to yield a 2.5:1:19 mass ratio of ceramic:polymer:salt. The powdered mixture was compressed under 2 metric tons for 1 min to form solid disks (final dimensions, 8 mm in diameter and 2 mm in height) using a Carver Press (Carver Inc., Wabash, IN). Compressed disks were exposed to high-pressure CO_2 gas (5.5 MPa) for at least 16 hours, followed by rapid pressure release to prompt polymer fusion. Salt particles were leached from scaffolds in distilled H_2O for 24 hours to generate HA-PLG composite scaffolds. Scaffolds were sterilized by 70% ethanol under gentle vacuum, followed by two rinses in sterile PBS.

Seeding BMA in perfusion bioreactors

Unprocessed human BMA was from Lonza [10 ml of aspirate from n = 3 donors (two males and one female; 21 to 26 years old; mean age, 23 ± 2.5 years)]. BMA was diluted 1:5 in PBS and pelleted by centrifugation at 1000*g*. Cells were incubated in a red blood cell lysis buffer (154.4 mM ammonium chloride, 10 mM potassium bicarbonate, and 97.3 mM EDTA tetrasodium salt) for 5 min at 37°C and washed with PBS, and viable cells were quantified using a Countess II Automated Cell Counter (Thermo Fisher Scientific). Culture medium was prepared with equal parts of α-MEM supplemented with 10% FBS and 1% P/S, Microvascular Endothelial Growth Medium-2 (EGM-2MV), and RPMI 1640 supplemented with 10% FBS and 1% P/S. Bioreactor seeding was performed as previously described (*16*, *47*, *48*). Briefly, scaffolds were installed into U-CUP flow perfusion bioreactors (CELLEC BIOTEK, Basel, Switzerland), and 10 ml of medium was injected into the bottom port. Medium was further supplemented with ECM (100 μg ml^{-1}) to produce ECM-coated scaffolds (Fig. 1A). Cells were resuspended in medium with ECM, and 2 ml of solution was injected as described (Fig. 1B). Bioreactors were perfused at a superficial velocity of 3 ml min^{-1} for 20 hours to seed the constructs (Fig. 1C). Scaffolds collected or implanted after the 20-hour seeding duration were referred to as naïve scaffolds (Fig. 1D). To generate preconditioned scaffolds, medium was refreshed after 20 hours and then every 2 to

3 days with osteogenic medium [culture medium supplemented with ascorbate 2-phosphate (50 μg ml^{-1}), 10 mM β-glycerophosphate, and 10 nM dexamethasone (all from Sigma-Aldrich)] for a total of 14 days (Fig. 1E).

Immunophenotype of entrapped cells

Entrapped cells were liberated from scaffolds through enzymatic and mechanical digestion. Scaffolds were washed with PBS, followed by perfusion of 12 ml of trypsin for 5 min at 37°C. Trypsin was retrieved from the bioreactors and added to an equal volume of medium. Scaffolds were removed from bioreactors, minced, and immersed in trypsin for an additional 5 min at 37°C in a tube rotator (Thermo Fisher Scientific, Santa Clara, CA) at 15 rpm. The immunophenotype of retrieved cells was determined using flow cytometry. Briefly, nonspecific binding was blocked by incubation in Protein Block (AB156024, Abcam, Cambridge, MA) for 20 min and then incubated with antibodies against CD31 (303110), CD45 (368518), CD34 (343623), CD90 (328112), and CD73 (344008) (all from BioLegend, San Diego, CA) per the manufacturer's instructions.

Gene expression and protein secretion

To interrogate osteogenic and proangiogenic gene expression, samples were collected in TRIzol Reagent (Invitrogen) for PCR analysis following the manufacturer's instructions. After RNA isolation, 600 ng of RNA was reverse-transcribed with the QuantiTect Reverse Transcription Kit (QIAGEN, Valencia, CA), and qPCR was performed using the QuantiFast Probe PCR Kit (QIAGEN) on a QuantStudio 5 system (Applied Biosystems). Primers and probes for housekeeping genes *RPL13* (Hs00744303_s1), *RUNX2* (Hs01047973_m1), *SP7* (Hs01866874_s1), *BGLAP* (Hs01587814_g1), *IBSP* (Hs00173720_m1), *COL1A1* (Hs00164004_m1), *BMP-2* (Hs00154192_m1), and *VEGF-A* (Hs00900055_m1) were purchased from Thermo Fisher Scientific. Amplification conditions were 95°C for 3 min, followed by 45 cycles at 95°C for 3 s and 60°C for 30 s. qPCR results were normalized to *RPL13* transcript levels to yield ΔC_t and cells from fresh BMA to yield $\Delta\Delta C_t$. Last, fold change in expression relative to the untreated and housekeeping gene was calculated using $2^{-\Delta\Delta Ct}$. Osteogenic and proangiogenic protein secretions were assessed by quantifying VEGF, OCN, and BMP-2 secretion with protein-specific ELISA kits per the manufacturer's instructions (R&D Systems, Minneapolis, MN).

RNA-seq library preparation was performed using Illumina TruSeq RNA Library Preparation Kit v2 (catalog no. RS-122-2002, Illumina), and single-end 75–base pair sequencing was performed using an Illumina NextSeq 500. Sequencing data quality was checked using FastQC software (www.bioinformatics.babraham.ac.uk/projects/fastqc/). Reads were mapped to the human genome (hg38) using STAR (*49*), and read counts per gene were determined using "featureCounts" from Rsubread package (*50*). Differentially expressed genes were identified using limma after voom normalization (*51*). A gene was considered as significantly differentially expressed when its false discovery rate–adjusted *P* value was <0.05 and fold change was >2. Gene ontology enrichment analysis was performed using ToppGene (*52*). Heatmaps were generated using the heatmap.2 function in "gplots" R package.

Histological analysis and SEM

Scaffolds were fixed in 10% formalin acetate overnight at 4°C, washed two times with water, soaked overnight in optimal cutting temperature (OCT) compound, frozen, and sectioned at 5 μm. Collagenous ECM was visualized with a picrosirius red stain using standard protocols, and the presence of OCN, an osteogenic ECM protein, was detected using a primary antibody against OCN (1:200; AB13420, Abcam).

Cell morphology was visualized with SEM (*35*, *47*). Scaffolds were fixed in freshly prepared Karnovsky's fixative solution overnight at 4°C, washed twice with water, bisected, and dehydrated in increasing concentrations of ethanol. Following dehydration, samples were critical point dried (Supercritical Autosamdri-931, Tousimis Research Corp., Rockville, MD), fixed to stubs with silver paste, sputter-coated with gold (Pelco SC-7 Auto Sputter Coater), and imaged using a scanning electron microscope (Quattro ESEM, Thermo Fisher Scientific, Newington, NH).

Evaluation of scaffold in rat orthotopic bone defect

Rats underwent bilateral calvarial osteotomies as previously described (*53*, *54*), and treatment of experimental animals was in accordance with University of California, Davis animal care guidelines and all National Institutes of Health animal handling procedures. Ten-week-old male nude rats (Taconic Biosciences, Germantown, NY) were anesthetized (3.0%) and maintained (1.5%) under an isoflurane/O_2 mixture delivered through a nose cone at 6 liters min^{-1}. A mid-longitudinal 15-mm skin incision was made on the dorsal surface of the cranium. The periosteum was completely cleared from the surface of the cranial bone by scraping. A trephine bur was used to create one circular 3.5-mm-diameter defect in the rat cranium on each side of the sagittal suture, and the full thickness (~1 mm) of the cranial bone was removed. Implants were generated with a final diameter of 3.5 mm using a biopsy punch and immediately placed directly into the osteotomy site—randomizing the side that received a cellular implant. Each animal received two implants: a naïve or preconditioned construct and an acellular control that had been exposed to perfusion culture for the same duration as its cellular counterpart (Fig. 1F). Animals were euthanized at 2 or 10 weeks after implantation, and calvariae were collected and fixed in 10% buffered formalin acetate for 1 day at 4°C. Samples were washed twice in deionized water to remove residual formalin acetate and preserved in 70% ethanol at 4°C until further processing.

Qualitative and quantitative 3D analyses of explants at 10 weeks were conducted using micro-CT (*28*, *47*). Explants were imaged (70 kilovolt peak, 114 μA, 300-ms integration time, average of three images) using a high-resolution micro-CT specimen scanner (mCT 35, Scanco Medical, Brüttisellen, Switzerland). Contiguous slices of 2048 pixels by 2048 pixels were imaged with 15-μm resolution and slice thickness (voxels). Serial tomograms were reconstructed from raw data of 1000 projections per 180° using a cone beam filtered back projection algorithm (*31*). The tomograms were calibrated to 0.0, 99.6, 200.0, 401.0, and 800.3 mg HA cm^{-3} concentrations of HA so that gray values of the images were converted to units of density in milligrams of HA per cubic centimeter. The entire defect was analyzed by selecting a 3.5-mm-diameter region of interest extending through the bone thickness. Material in the reconstructed images was partitioned by a threshold of 256 to 3000 mg HA cm^{-3} to discriminate between mineralized and unmineralized tissue. After thresholding, the image noise was reduced using a low-pass Gaussian filter (σ = 0.8, support = 1). BV fraction [BV/TV (total volume)] was determined by dividing the number of pixels representing bone tissue (BV) by the number of pixels in the cylindrical segment (TV).

After micro-CT analysis, explants were demineralized in Calci-Clear (National Diagnostics, Atlanta, GA) for 7 days, washed twice in water, dehydrated, paraffin-embedded, and sectioned at 5 μm thickness. To visualize tissue formation and morphology, sections were stained with H&E and Masson's trichrome. Blood vessel density at 10 days was quantified using H&E-stained cross sections by counting circular structures with well-defined lumens. To detect the persistence of human ECs, sections were immunostained with a primary antibody against human CD31 (1:50; AB28364, Abcam). To detect osteogenic human MSCs, sections were immunostained with a primary antibody against human DLX5 (10 μg ml^{-1}; AF6710, R&D Systems), stained using a NorthernLights 557–conjugated secondary antibody (1:200; NL010, R&D Systems), and counter-stained with 4′,6-diamidino-2-phenylindole (2 μg ml^{-1}; D1306, Thermo Fisher Scientific).

Laser Doppler perfusion imaging

Blood flow was measured on anesthetized animals 1, 7, 14, 21, 28, 35, and 70 days after surgery using a PeriScan PIM 3 laser Doppler blood perfusion imager (Perimed, Stockholm, Sweden) (*32*). The hair covering the surgical site was removed the day before scanning, and the calvariae were cleaned using alcohol wipes immediately before data acquisition. Perfusion measurements were obtained from a circular region of interest superimposed over the defect.

Statistical analysis

Data are presented as means ± SD of $n = 3$ to 6 replicates from two to three biological donors unless otherwise stated. Statistical analyses between two groups were performed with Student's unpaired t tests and between three or more groups with one-way analysis of variance (ANOVA), followed by Tukey's multiple comparison post hoc test (GraphPad Prism 8.0, San Diego, CA) to determine significance ($P < 0.05$). Significance between groups is denoted with asterisks. A lack of significance between groups is indicated with "ns" and a line bridging nonsignificant groups. Correlations between bivariate parameters were modeled using simple linear least-squares regression analysis, and statistical analysis was performed using JMP software (SAS, Cary, NC).

SUPPLEMENTARY MATERIALS

Supplementary material for this article is available at http://advances.sciencemag.org/cgi/content/full/6/7/eaay2387/DC1

Fig. S1. Genes associated with immune system development are down-regulated with increasing time in culture.

Fig. S2. HA is degraded and removed from composite scaffolds during preconditioning in the bioreactor.

Fig. S3. Preconditioned scaffolds exhibit improved integration with host bone.

Table S1. Genes associated with immune system development down-regulated in preconditioned compared to naïve constructs.

Table S2. Genes associated with osteoblast differentiation and bone development up-regulated in preconditioned compared to naïve constructs.

Table S3. Genes associated with vasculature development up-regulated in preconditioned compared to naïve constructs.

View/request a protocol for this paper from *Bio-protocol*.

REFERENCES AND NOTES

1. M. Alvarez-Viejo, Y. Menendez-Menendez, M. A. Blanco-Gelaz, A. Ferrero-Gutierrez, M. A. Fernandez-Rodriguez, J. Gala, J. Otero-Hernandez, Quantifying mesenchymal stem cells in the mononuclear cell fraction of bone marrow samples obtained for cell therapy. *Transplant. Proc.* **45**, 434–439 (2013).
2. C. Hu, L. Li, Preconditioning influences mesenchymal stem cell properties in vitro and in vivo. *J. Cell. Mol. Med.* **22**, 1428–1442 (2018).
3. Z. Yang, J. Concannon, K. S. Ng, K. Seyb, L. J. Mortensen, S. Ranganath, F. Gu, O. Levy, Z. Tong, K. Martyn, W. Zhao, C. P. Lin, M. A. Glicksman, J. M. Karp, Tetrandrine identified in a small molecule screen to activate mesenchymal stem cells for enhanced immunomodulation. *Sci. Rep.* **6**, 30263 (2016).
4. J. Beegle, K. Lakatos, S. Kalomoiris, H. Stewart, R. R. Isseroff, J. A. Nolta, F. A. Fierro, Hypoxic preconditioning of mesenchymal stromal cells induces metabolic changes, enhances survival, and promotes cell retention in vivo. *Stem Cells* **33**, 1818–1828 (2015).
5. I. Rosová, M. Dao, B. Capoccia, D. Link, J. A. Nolta, Hypoxic preconditioning results in increased motility and improved therapeutic potential of human mesenchymal stem cells. *Stem Cells* **26**, 2173–2182 (2008).
6. S. S. Ho, B. P. Hung, N. Heyrani, M. A. Lee, J. K. Leach, Hypoxic preconditioning of mesenchymal stem cells with subsequent spheroid formation accelerates repair of segmental bone defects. *Stem Cells* **36**, 1393–1403 (2018).
7. A. I. Hoch, R. Duhr, N. Di Maggio, A. Mehrkens, M. Jakob, D. Wendt, Expansion of bone marrow mesenchymal stromal cells in perfused 3D ceramic scaffolds enhances in vivo bone formation. *Biotechnol. J.* **12**, 1700071 (2017).
8. A. Scherberich, R. Galli, C. Jaquiery, J. Farhadi, I. Martin, Three-dimensional perfusion culture of human adipose tissue-derived endothelial and osteoblastic progenitors generates osteogenic constructs with intrinsic vascularization capacity. *Stem Cells* **25**, 1823–1829 (2007).
9. A. Mehrkens, F. Saxer, S. Güven, W. Hoffmann, A. M. Müller, M. Jakob, F. E. Weber, I. Martin, A. Scherberich, Intraoperative engineering of osteogenic grafts combining freshly harvested, human adipose-derived cells and physiological doses of bone morphogenetic protein-2. *Eur. Cell. Mater.* **24**, 308–319 (2012).
10. R. O. Hynes, The extracellular matrix: Not just pretty fibrils. *Science* **326**, 1216–1219 (2009).
11. T. H. Barker, The role of ECM proteins and protein fragments in guiding cell behavior in regenerative medicine. *Biomaterials* **32**, 4211–4214 (2011).
12. C. D. Reyes, T. A. Petrie, A. J. García, Mixed extracellular matrix ligands synergistically modulate integrin adhesion and signaling. *J. Cell. Physiol.* **217**, 450–458 (2008).
13. N. Sadr, B. E. Pippenger, A. Scherberich, D. Wendt, S. Mantero, I. Martin, A. Papadimitropoulos, Enhancing the biological performance of synthetic polymeric materials by decoration with engineered, decellularized extracellular matrix. *Biomaterials* **33**, 5085–5093 (2012).
14. R. A. Thibault, A. G. Mikos, F. K. Kasper, Protein and mineral composition of osteogenic extracellular matrix constructs generated with a flow perfusion bioreactor. *Biomacromolecules* **12**, 4204–4212 (2011).
15. P. E. Bourgine, T. Klein, A. M. Paczulla, T. Shimizu, L. Kunz, K. D. Kokkaliaris, D. L. Coutu, C. Lengerke, R. Skoda, T. Schroeder, I. Martin, In vitro biomimetic engineering of a human hematopoietic niche with functional properties. *Proc. Natl. Acad. Sci. U.S.A.* **115**, E5688–E5695 (2018).
16. J. N. Harvestine, A. M. Saiz Jr., J. K. Leach, Cell-secreted extracellular matrix influences cellular composition sequestered from unprocessed bone marrow aspirate for osteogenic grafts. *Biomater. Sci.* **7**, 2091–2101 (2019).
17. N. Samee, V. Geoffroy, C. Marty, C. Schiltz, M. Vieux-Rochas, G. Levi, M. C. de Vernejoul, Dlx5, a positive regulator of osteoblastogenesis, is essential for osteoblast-osteoclast coupling. *Am. J. Pathol.* **173**, 773–780 (2008).
18. M. T. Houdek, C. C. Wyles, M. S. Collins, B. M. Howe, A. Terzic, A. Behfar, R. J. Sierra, Stem cells combined with platelet-rich plasma effectively treat corticosteroid-induced osteonecrosis of the hip: A prospective study. *Clin. Orthop. Relat. Res.* **476**, 388–397 (2018).
19. A. Gobbi, G. Karnatzikos, C. Scotti, V. Mahajan, L. Mazzucco, B. Grigolo, One-step cartilage repair with bone marrow aspirate concentrated cells and collagen matrix in full-thickness knee cartilage lesions: Results at 2-year follow-up. *Cartilage* **2**, 286–299 (2011).
20. P. Hernigou, Y. Homma, C. H. Flouzat Lachaniette, A. Poignard, J. Allain, N. Chevallier, H. Rouard, Benefits of small volume and small syringe for bone marrow aspirations of mesenchymal stem cells. *Int. Orthop.* **37**, 2279–2287 (2013).
21. S. Güven, A. Mehrkens, F. Saxer, D. J. Schaefer, R. Martinetti, I. Martin, A. Scherberich, Engineering of large osteogenic grafts with rapid engraftment capacity using mesenchymal and endothelial progenitors from human adipose tissue. *Biomaterials* **32**, 5801–5809 (2011).
22. V. Bunpetch, Z.-Y. Zhang, X. Zhang, S. Han, P. Zongyou, H. Wu, O. Hong-Wei, Strategies for MSC expansion and MSC-based microtissue for bone regeneration. *Biomaterials* **196**, 67–79 (2019).
23. A. L. Russell, R. C. Lefavor, A. C. Zubair, Characterization and cost–benefit analysis of automated bioreactor-expanded mesenchymal stem cells for clinical applications. *Transfusion* **58**, 2374–2382 (2018).
24. G. N. Bancroft, V. I. Sikavitsas, J. van den Dolder, T. L. Sheffield, C. G. Ambrose, J. A. Jansen, A. G. Mikos, Fluid flow increases mineralized matrix deposition in 3D perfusion culture of marrow stromal osteoblasts in a dose-dependent manner. *Proc. Natl. Acad. Sci. U.S.A.* **99**, 12600–12605 (2002).

25. V. I. Sikavitsas, G. N. Bancroft, H. L. Holtorf, J. A. Jansen, A. G. Mikos, Mineralized matrix deposition by marrow stromal osteoblasts in 3D perfusion culture increases with increasing fluid shear forces. *Proc. Natl. Acad. Sci. U.S.A.* **100**, 14683–14688 (2003).
26. F. Zhao, B. van Rietbergen, K. Ito, S. Hofmann, Flow rates in perfusion bioreactors to maximise mineralisation in bone tissue engineering in vitro. *J. Biomech.* **79**, 232–237 (2018).
27. A. I. Hoch, B. Y. Binder, D. C. Genetos, J. K. Leach, Differentiation-dependent secretion of proangiogenic factors by mesenchymal stem cells. *PLOS ONE* **7**, e35579 (2012).
28. A. I. Hoch, V. Mittal, D. Mitra, N. Vollmer, C. A. Zikry, J. K. Leach, Cell-secreted matrices perpetuate the bone-forming phenotype of differentiated mesenchymal stem cells. *Biomaterials* **74**, 178–187 (2016).
29. R. L. Dahlin, J. G. Gershovich, F. K. Kasper, A. G. Mikos, Flow perfusion co-culture of human mesenchymal stem cells and endothelial cells on biodegradable polymer scaffolds. *Ann. Biomed. Eng.* **42**, 1381–1390 (2014).
30. C. S. Bahney, D. P. Hu, A. J. Taylor, F. Ferro, H. M. Britz, B. Hallgrimsson, B. Johnstone, T. Miclau, R. S. Marcucio, Stem cell–derived endochondral cartilage stimulates bone healing by tissue transformation. *J. Bone Miner. Res.* **29**, 1269–1282 (2014).
31. J. He, D. C. Genetos, J. K. Leach, Osteogenesis and trophic factor secretion are influenced by the composition of hydroxyapatite/poly(lactide-co-glycolide) composite scaffolds. *Tissue Eng. Part A* **16**, 127–137 (2010).
32. D. Kaigler, Z. Wang, K. Horger, D. J. Mooney, P. H. Krebsbach, VEGF scaffolds enhance angiogenesis and bone regeneration in irradiated osseous defects. *J. Bone Miner. Res.* **21**, 735–744 (2006).
33. R. M. Eman, H. A. Meijer, F. C. Öner, W. J. Dhert, J. Alblas, Establishment of an early vascular network promotes the formation of ectopic bone. *Tissue Eng. Part A* **22**, 253–262 (2016).
34. X. Liu, W. Chen, C. Zhang, W. Thein-Han, K. Hu, M. A. Reynolds, C. Bao, P. Wang, L. Zhao, H. H. K. Xu, Co-seeding human endothelial cells with human-induced pluripotent stem cell-derived mesenchymal stem cells on calcium phosphate scaffold enhances osteogenesis and vascularization in rats. *Tissue Eng. Part A* **23**, 546–555 (2017).
35. J. N. Harvestine, N. L. Vollmer, S. S. Ho, C. A. Zikry, M. A. Lee, J. K. Leach, Extracellular matrix-coated composite scaffolds promote mesenchymal stem cell persistence and osteogenesis. *Biomacromolecules* **17**, 3524–3531 (2016).
36. J. N. Harvestine, H. Orbay, J. Y. Chen, D. E. Sahar, J. K. Leach, Cell-secreted extracellular matrix, independent of cell source, promotes the osteogenic differentiation of human stromal vascular fraction. *J. Mater. Chem. B* **6**, 4104–4115 (2018).
37. N. Datta, Q. P. Pham, U. Sharma, V. I. Sikavitsas, J. A. Jansen, A. G. Mikos, In vitro generated extracellular matrix and fluid shear stress synergistically enhance 3D osteoblastic differentiation. *Proc. Natl. Acad. Sci. U.S.A.* **103**, 2488–2493 (2006).
38. K. C. Murphy, R. S. Stilhano, D. Mitra, D. Zhou, S. Batarni, E. A. Silva, J. K. Leach, Hydrogel biophysical properties instruct coculture-mediated osteogenic potential. *FASEB J.* **30**, 477–486 (2016).
39. A. Shafiee, J. Patel, H. Y. Wong, P. Donovan, D. W. Hutmacher, N. M. Fisk, K. Khosrotehrani, Priming of endothelial colony-forming cells in a mesenchymal niche improves engraftment and vasculogenic potential by initiating mesenchymal transition orchestrated by NOTCH signaling. *FASEB J.* **31**, 610–624 (2017).
40. R.-Z. Lin, R. Moreno-Luna, D. Li, S.-C. Jaminet, A. K. Greene, J. M. Melero-Martin, Human endothelial colony-forming cells serve as trophic mediators for mesenchymal stem cell engraftment via paracrine signaling. *Proc. Natl. Acad. Sci. U.S.A.* **111**, 10137–10142 (2014).
41. J. Dai, A. B. Rabie, VEGF: An essential mediator of both angiogenesis and endochondral ossification. *J. Dent. Res.* **86**, 937–950 (2007).
42. T. L. Clemens, H. Tang, S. Maeda, R. A. Kesterson, F. Demayo, J. W. Pike, C. M. Gundberg, Analysis of osteocalcin expression in transgenic mice reveals a species difference in vitamin D regulation of mouse and human osteocalcin genes. *J. Bone Miner. Res.* **12**, 1570–1576 (1997).
43. V. Shalhoub, F. Aslam, E. Breen, A. van Wijnen, R. Bortell, G. S. Stein, J. L. Stein, J. B. Lian, Multiple levels of steroid hormone-dependent control of osteocalcin during osteoblast differentiation: Glucocorticoid regulation of basal and vitamin D stimulated gene expression. *J. Cell. Biochem.* **69**, 154–168 (1998).
44. D. P. Hu, F. Ferro, F. Yang, A. J. Taylor, W. Chang, T. Miclau, R. S. Marcucio, C. S. Bahney, Cartilage to bone transformation during fracture healing is coordinated by the invading vasculature and induction of the core pluripotency genes. *Development* **144**, 221–234 (2017).
45. M. L. Decaris, J. K. Leach, Design of experiments approach to engineer cell-secreted matrices for directing osteogenic differentiation. *Ann. Biomed. Eng.* **39**, 1174–1185 (2011).
46. M. L. Decaris, A. Mojadedi, A. Bhat, J. K. Leach, Transferable cell-secreted extracellular matrices enhance osteogenic differentiation. *Acta Biomater.* **8**, 744–752 (2012).
47. D. Mitra, J. Whitehead, O. W. Yasui, J. K. Leach, Bioreactor culture duration of engineered constructs influences bone formation by mesenchymal stem cells. *Biomaterials* **146**, 29–39 (2017).
48. D. Wendt, A. Marsano, M. Jakob, M. Heberer, I. Martin, Oscillating perfusion of cell suspensions through three-dimensional scaffolds enhances cell seeding efficiency and uniformity. *Biotechnol. Bioeng.* **84**, 205–214 (2003).
49. A. Dobin, T. R. Gingeras, Mapping RNA-seq reads with STAR. *Curr. Protoc. Bioinformatics* **51**, 11.14.1–11.14.19 (2015).
50. Y. Liao, G. K. Smyth, W. Shi, featureCounts: An efficient general purpose program for assigning sequence reads to genomic features. *Bioinformatics* **30**, 923–930 (2014).
51. C. W. Law, Y. Chen, W. Shi, G. K. Smyth, voom: Precision weights unlock linear model analysis tools for RNA-seq read counts. *Genome Biol.* **15**, R29 (2014).
52. J. Chen, E. E. Bardes, B. J. Aronow, A. G. Jegga, ToppGene Suite for gene list enrichment analysis and candidate gene prioritization. *Nucleic Acids Res.* **37**, W305–W311 (2009).
53. W. K. Cheung, D. M. Working, L. D. Galuppo, J. K. Leach, Osteogenic comparison of expanded and uncultured adipose stromal cells. *Cytotherapy* **12**, 554–562 (2010).
54. K. C. Murphy, M. L. Hughbanks, B. Y. K. Binder, C. B. Vissers, J. K. Leach, Engineered fibrin gels for parallel stimulation of mesenchymal stem cell proangiogenic and osteogenic potential. *Ann. Biomed. Eng.* **43**, 2010–2021 (2015).

Acknowledgments

Funding: This work was supported by grants from the California Institute for Regenerative Medicine (grant number RT3-07981), the NIH (NIDCR DE025899), and the UC Davis Veterinary Institute for Regenerative Cures to J.K.L. The content is solely the responsibility of the authors and does not necessarily represent the official views of the NIH, CIRM, or any other agency of the State of California. The funders had no role in the decision to publish or preparation of the manuscript. J.N.H. received support from the National Defense Science and Engineering Graduate Fellowship (32 CFR 168a), Schwall Fellowship in Medical Research, and Achievement Rewards for College Scientists (ARCS) Foundation. T.G.F. received support from the American Heart Association Postdoctoral Fellowship (19POST34460034). A.S., N.R.H., and G.G.L. performed work under the auspices of the U.S. Department of Energy by the Lawrence Livermore National Laboratory under contract DE-AC52-07NA27344. **Author contributions:** J.N.H., T.G.-F., A.S., N.R.H., and G.G.L.: Conception and design of experiments, data collection and assembly, data analysis and interpretation, and manuscript composition. D.C.G.: Data analysis and interpretation and manuscript composition. J.K.L.: Conception and design of experiments, data analysis and interpretation, manuscript composition, and administrative support. **Competing interests:** The authors declare that they have no competing interests. **Data and materials availability:** All data needed to evaluate the conclusions in the paper are present in the paper and/or the Supplementary Materials. Additional data related to this paper may be requested from the authors.

Submitted 31 May 2019
Accepted 26 November 2019
Published 12 February 2020
10.1126/sciadv.aay2387

Citation: J. N. Harvestine, T. Gonzalez-Fernandez, A. Sebastian, N. R. Hum, D. C. Genetos, G. G. Loots, J. K. Leach, Osteogenic preconditioning in perfusion bioreactors improves vascularization and bone formation by human bone marrow aspirates. *Sci. Adv.* **6**, eaay2387 (2020).